Journal of Medicinal Chemistry

Article

pubs.acs.org/jmc

Fluorine Modulates Species Selectivity in the Triazolopyrimidine Class of *Plasmodium falciparum* Dihydroorotate Dehydrogenase Inhibitors

Xiaoyi Deng,[†] Sreekanth Kokkonda,[‡] Farah El Mazouni,[†] John White,[‡] Jeremy N. Burrows,[∥] Werner Kaminsky,[‡] Susan A. Charman,[§] David Matthews,[∥] Pradipsinh K. Rathod,[‡] and Margaret A. Phillips*[,†]

[†]Department of Pharmacology, University of Texas Southwestern Medical Center at Dallas, 6001 Forest Park Boulevard, Dallas, Texas 75390-9041, United States

[‡]Departments of Chemistry and Global Health, University of Washington, Seattle, Washington 98195, United States

[§]Centre for Drug Candidate Optimisation, Monash Institute of Pharmaceutical Sciences, Monash University−Parkville, Parkville, Victoria 3052, Australia

[∥]Medicines for Malaria Venture, Geneva 1215, Switzerland

Supporting Information

ABSTRACT: Malaria is one of the most serious global infectious diseases. The pyrimidine biosynthetic enzyme *Plasmodium falciparum* dihydroorotate dehydrogenase (*Pf*DHODH) is an important target for antimalarial chemotherapy. We describe a detailed analysis of protein−ligand interactions between DHODH and a triazolopyrimidine-based inhibitor series to explore the effects of fluorine on affinity and species selectivity. We show that increasing fluorination dramatically increases binding to mammalian DHODHs, leading to a loss of species selectivity. Triazolopyrimidines bind *Plasmodium* and mammalian DHODHs in overlapping but distinct binding sites. Key hydrogen-bond and stacking interactions underlying strong binding to *Pf*DHODH are absent in the mammalian enzymes. Increasing fluorine substitution leads to an increase in the entropic contribution to binding, suggesting that strong binding to mammalian DHODH is a consequence of an enhanced hydrophobic effect upon binding to an apolar pocket. We conclude that hydrophobic interactions between fluorine and hydrocarbons provide significant binding energy to protein−ligand interactions. Our studies define the requirements for species-selective binding to *Pf*DHODH and show that the triazolopyrimidine scaffold can alternatively be tuned to inhibit human DHODH, an important target for autoimmune diseases.

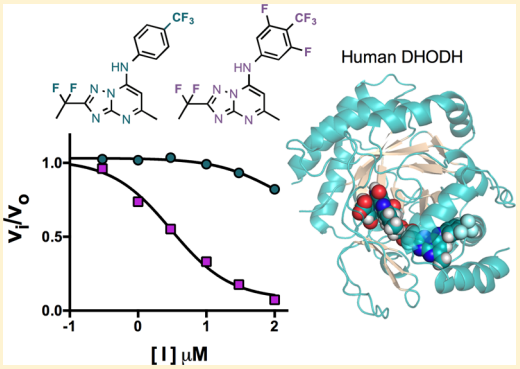

INTRODUCTION

Malaria remains one of the most devastating global infectious diseases. It is endemic in over 90 countries, and it is estimated that it causes 630 000 deaths annually (World Malaria Report 2013), with pregnant women and children under 5 being the most susceptible to severe disease.[1] Despite extensive efforts to develop vaccines, no effective strategy has emerged, with the leading candidate, RTS,S, providing only modest protection in phase III trials.[2,3] Drug therapy remains the only viable option for prevention and treatment, and it is critical to ongoing efforts to eradicate the disease.[4] The introduction of artemisinin combination therapy and improved vector control are credited with recent reductions in the number of global malaria cases.[5] However, artemisinin resistance is emerging in Asia and threatens to derail progress,[6−9] mirroring past set backs caused by the emergence of resistance to other key therapies (e.g., chloroquine and pyrimethamine[10]). To combat the propensity for malaria to develop resistance, it is essential that new therapeutics continue to be developed.[11]

Recent efforts have led to a robust pipeline of potential new antimalarials at different stages of development ranging from early lead optimization to clinical trials.[12] Our group used a target-based drug discovery strategy that led to the identification of dihydroorotate dehydrogenase (DHODH) as a new drug target for the treatment of malaria.[13] DHODH catalyzes the flavin mononucleotide (FMN)-dependent oxidation of dihydroorotate to orotic acid, an essential step in de novo pyrimidine biosynthesis.[13] De novo pyrimidine biosynthesis is essential to the malaria parasites because the parasites lack salvage pathways that provide an alternative source of pyrimidines. Both pathways are present in most other

Received: March 26, 2014
Published: May 7, 2014

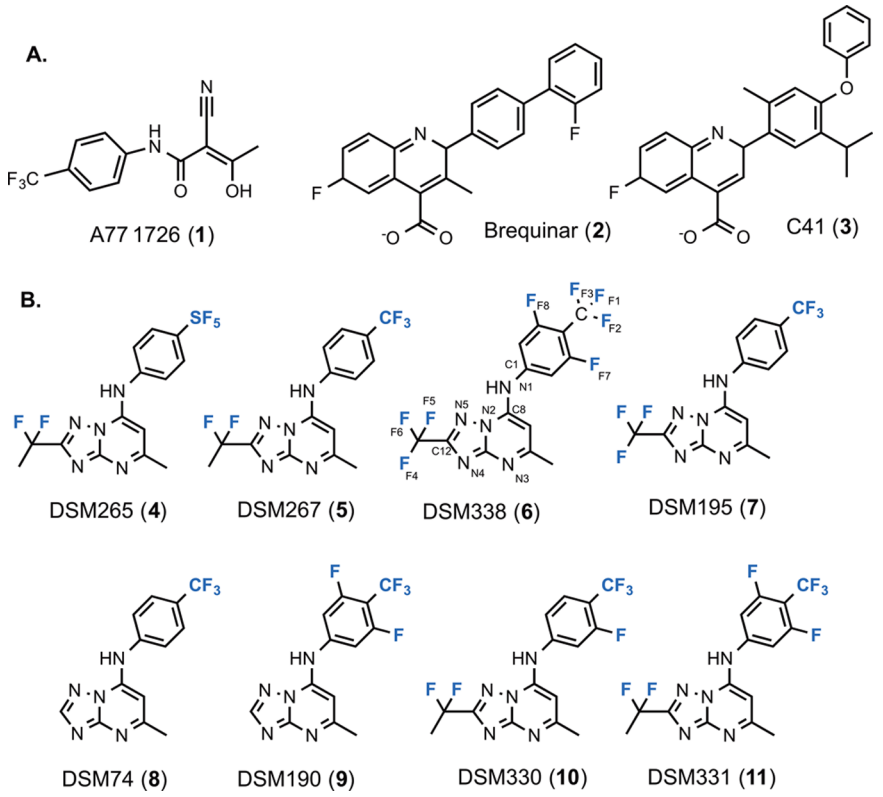

Figure 1. Structures of DHODH inhibitors. (A) Inhibitors of human DHODH. (B) Triazolopyrmidine-based DHODH inhibitors. Atom numbers for **6** are shown on the basis of the numbers assigned in the coordinates for the PDB database.

organisms, including humans. DHODH belongs to a diverse β/α-barrel fold enzyme family that includes mitochondrial enzymes that utilize ubiquinone (CoQ) as the final electron acceptor and cytoplasmic enzymes that use fumarate instead. Both human and malaria DHODH are mitochondrial enzymes, but X-ray structural analysis has shown that although the overall fold is well-conserved, the presumptive CoQ binding site is variable between species.[14−17] An inhibitor of human DHODH (*Hs*DHODH) (teriflunomide (A77 1726) (**1**), the active metabolite of leflunomide (Figure 1)) is clinically approved for the treatment of rheumatoid arthritis and multiple sclerosis, and a number of compounds have been described that either bind potently to the human enzyme (e.g., brequinar (**2**) and C41 (**3**)) or selectively inhibit DHODH from various microbial species, demonstrating that DHODH is a druggable target.[13,18,19]

Plasmodium falciparum DHODH is the target of a triazolopyrimidine-based compound series with selective and potent antimalarial activity. These compounds are composed of a triazolopyrimidine core linked via the amine to a substituted aniline (Figure 1). We identified the triazolopyrimidines as potent and selective *Pf*DHODH inhibitors by an enzyme-based high-throughput screen.[13] Subsequent lead optimization led to the identification of inhibitors with nanomolar affinity against *Pf*DHODH, with good in vivo antimalarial activity and excellent pharmacological properties.[20−23] A compound from the triazolopyrimidine series (DSM265 (**4**); Figure 1)[20] is currently in phase I human clinical trials for the treatment of malaria (www.mmv.org) and is the first *Pf*DHODH inhibitor to advance to this stage of development. A key factor in the safety of DHODH inhibitors for the treatment of malaria is that inhibitors like **4** display strong species selectivity for parasite DHODH over the human enzyme. High-resolution crystal structures of *Pf*DHODH−inhibitor complexes showed that the binding site of close analogues to **4** has a number of amino acid differences between *Pf*DHODH and *Hs*DHODH that were postulated to account for selectivity.[15,20]

The pharmacologic properties of the triazolopyrimidine series were optimized by the introduction of fluorocarbons. We found that *para*-substituted anilines form strong interactions in the hydrophobic site of the inhibitor binding pocket, with hydrophobic groups like CF_3 and SF_5 providing the best combination of potency and metabolic stability.[15,20−22,24] The addition of fluorine-bearing substituents to the aniline ring was, in fact, key to improving metabolic stability. A second key discovery was that the addition of difluoroethyl or trifluoromethyl to the triazolopyrimidine ring (C12 position, Figure 1) led to improved potency and to the discovery of the development candidate.

Flourine has several unique properties that make it a critical player in drug design.[25,26] The utility of fluorine to improve metabolic stability is well-documented; however, its contributions to the energetics of ligand binding are poorly understood. In the triazolopyrimidine series, the fluoro-substituted alkyl groups were significantly more potent than the analogous non-fluorinated alkyl groups (ethyl or methyl),[20−23] suggesting that the unique properties of fluorine contributed to potency, either potentially through influencing the electronics of the triazolopyrimidine ring or by providing for better hydrophobic interactions in the binding pocket. The addition of *meta*-fluorines to compounds with *para*-CF_3 aniline further improved plasma exposure and provided a modest boost in potency toward *Pf*DHODH;[21,22] however, this substitution was not tested in the context of the fully optimized triazolopyrimidines

dx.doi.org/10.1021/jm500481t | *J. Med. Chem.* 2014, 57, 5381−5394

Table 1. Steady-State Kinetic Analysis of Inhibitor Species Selectivity and Whole-Cell *P. falciparum* Activity[a]

		IC_{50} μM					
inhibitor	calcd pK_a (N1)	*P. falciparum* 3D7 cells	*Pf*DHODH	*Hs*DHODH	rDHODH	mDHODH	dDHODH
8	18.5	0.26 (0.16−0.43)	0.27 ± 0.025	>100	>100	>100	>100
9	17.0	0.22[b]	0.13[b]	>100	37 (26−48)	>30	>100
7	18.4	0.0063 (5.8−6.8)	0.035 (0.025−0.050)	>100	3.5 (3.2−3.9)	9.7 (7.4−13)	86 (70−100)
5	18.4	0.0036 (0.0026−0.0049)	0.046 (0.027−0.078)	>100	7.2 (5.3−9.8)	24 (16−37)	>100
10	17.7	0.0039 (0.0032−0.0046)	0.035 (0.025−0.050)	17 (9.7−24)	0.80 (0.70−0.93)	1.6 (1.3−2.0)	7.2 (6.2−8.3)
11	16.9	0.012 (0.011−0.013)	0.020 (0.01−0.03)	2.1 (1.5−2.8)	0.13 (0.12−0.15)	0.18 (0.16−0.21)	0.70 (0.6−0.8)
6	16.9	0.0018 (0.0016−0.0020)	0.022 (0.014−0.34)	1.6 (1.2−2.3)	0.049 (0.037−0.06)	0.088 (0.07−0.1)	0.32 (0.26−0.38)
1	NA	nd	3.9 (3.2−4.7)	0.44 (0.37−0.52)	0.018 (0.013−0.024)	0.15 (0.14−0.17)	0.32 (0.27−0.37)

[a]Compounds are ordered on the basis of decreasing species selectivity. The 95% confidence interval is displayed in parentheses. The data set included three replicates for each inhibitor concentration used in the fit. [b]Data taken from ref 22. *Pf*$DHODH_{158-569}$, human $DHODH_{30-396}$, mouse $DHODH_{30-396}$, rat $DHODH_{30-396}$, and dog $DHODH_{48-414}$ expression constructs were used for the study. Solubility limited the collection of data above concentrations of 100 μM. Data were collected using the DCIP assay.

that included fluoro alkyl groups at C12 of the triazolopyrimidine ring (e.g., **4** and DSM267 (**5**); Figure 1).

Herein, we explore the effects of fluorine on the potency and species selectivity of the triazolopyrimidine class of *Pf*DHODH inhibitors. Surprisingly, we found that addition of *meta*-fluorines to the aniline ring had a profound differential impact on species selectivity, particularly within the context of fluoro alkyl groups at C12. These compounds are potent inhibitors of *Pf*DHODH; however, they also show substantial inhibition of mammalian DHODHs. X-ray structures of an analogue from the series that contains two *meta*-fluorines (DSM338 (**6**); Figure 1) were solved in complex with *Pf*DHODH, *Hs*DHODH, and rat DHODH. Prior data had suggested that a suitable binding pocket would not be formed on the mammalian enzymes. These current structures show that a binding site is present but that it is inherently lower affinity than the binding site on *Pf*DHODH. The triazolopyrimidines bind to *Pf*DHODH and the mammalian enzymes in overlapping but distinct binding modes. For *Pf*DHODH, a key H-bond formed between an inhibitor amine (N1) and an active site His (H185), and two edge-to-face stacking interactions are important contributors to high-affinity binding. These interactions are inaccessible on the mammalian enzymes because of differing binding-modes, and they likely underlie the strong species selectivity of analogues in the series. The addition of extra fluorines into the system increases the hydrophobicity of the compounds, leading to more potent binding to the mammalian enzymes. The majority of the close fluorine protein contacts in all three structures occur with aliphatic amino acids. Site-directed mutagenesis, isothermal titration calorimetry, and small molecule crystallography were used to probe the nature of the binding site interactions. Mutation of two Leu residues positioned on either side of the *meta*-fluorines in human DHODH decreased binding, whereas increasing fluorine substitution led to an increase in the entropic contribution of binding to both the parasite and mammalian enzymes. We conclude that hydrophobic interactions between fluorine and hydrocarbons, directly and indirectly, can provide significant binding energy to protein−ligand interactions.

RESULTS

Effect of *meta*-Fluorine on Species Selectivity of Triazolopyrimidine-Based *Pf*DHODH Inhibitors. We previously reported the synthesis and activity of triazolopyrimidine analogues **5**, DSM195 (**7**), DSM74 (**8**), and DSM190 (**9**), which contain *para*-CF_3 aniline as a key component of their structures (Figure 1).[15,20,21] Herein, we synthesized three additional analogues (DSM330 (**10**), DSM331 (**11**), and **6**; Figure 1) containing *meta*-fluorines on the aniline ring. These compounds test the effect of combining this modification with the fluoroalkyl modification at C12 on the triazolopyrimidine ring, which was used to optimize the potency of the series (e.g., **4** and **5**). We evaluated the activity of the new analogues on *Pf*DHODH and *Hs*DHODH as well as against *P. falciparum* 3D7 cells in whole-cell assays (Table 1). Similar to **5** and **7**, the new analogues were potent inhibitors of *Pf*DHODH (IC_{50} 20−40 nM) and of *P. falciparum* growth (IC_{50} 2−12 nM). The addition of both *meta*-fluorines led to a modest 2−3-fold improvement in potency against *Pf*DHODH and the parasite in comparison to that of **5**. However, unexpectedly, and unlike **5**, which did not inhibit the human enzyme, these new analogues showed considerable activity against *Hs*DHODH (IC_{50} 2−20 μM) (Table 1). The addition of a single *meta*-fluorine decreased the IC_{50} by >5-fold, whereas two *meta*-fluorines had an even more profound effect, leading to a >50-fold more potent inhibition of *Hs*DHODH.

Because the development of any compound for clinical use would require toxicology studies in rodents and dog, we next cloned and expressed DHODH from mouse, rat, and dog to evaluate selectivity against these enzymes (Table 1). Compound **8** showed full selectivity and did not inhibit any of the mammalian enzymes, whereas the other analogues with additional fluorines all showed activity against the rodent enzymes and, to a lesser extent, the dog enzyme. Unlike for *Hs*DHODH, addition of trifluoromethyl or difluoroethyl to the C12 position led to a >5−25-fold more potent inhibition against rat and mouse DHODH (**8** vs **7** or **5**), whereas the addition of *meta*-fluorines to the aniline ring had even more profound effects on species selectivity. Comparison of compounds **8** to **9**, **7** to **6**, or **5** to **10** and **11** showed that a single *meta*-fluorine increased the affinity toward the mammalian enzymes by 5−10-fold, whereas two *meta*-fluorines led to a 50−100-fold increase in potency. The two compounds with *meta*-fluorines on the aniline ring, **6** and **11**, showed potency in the same range as the clinically used human DHODH inhibitor **1**, with the IC_{50}'s within 5-fold for *Hs*DHODH and similar or better for the rodent enzymes (Table 1). Compounds in the series were most inhibitory to the rodent enzymes, with the rank order of potency against mammalian DHODHs observed to be rat > mouse > dog ≫ human for all tested analogues. The effect of adding the *meta*-fluorines alone was similar for all of the mammalian enzymes tested; however, for the rodent

dx.doi.org/10.1021/jm500481t | J. Med. Chem. 2014, 57, 5381−5394

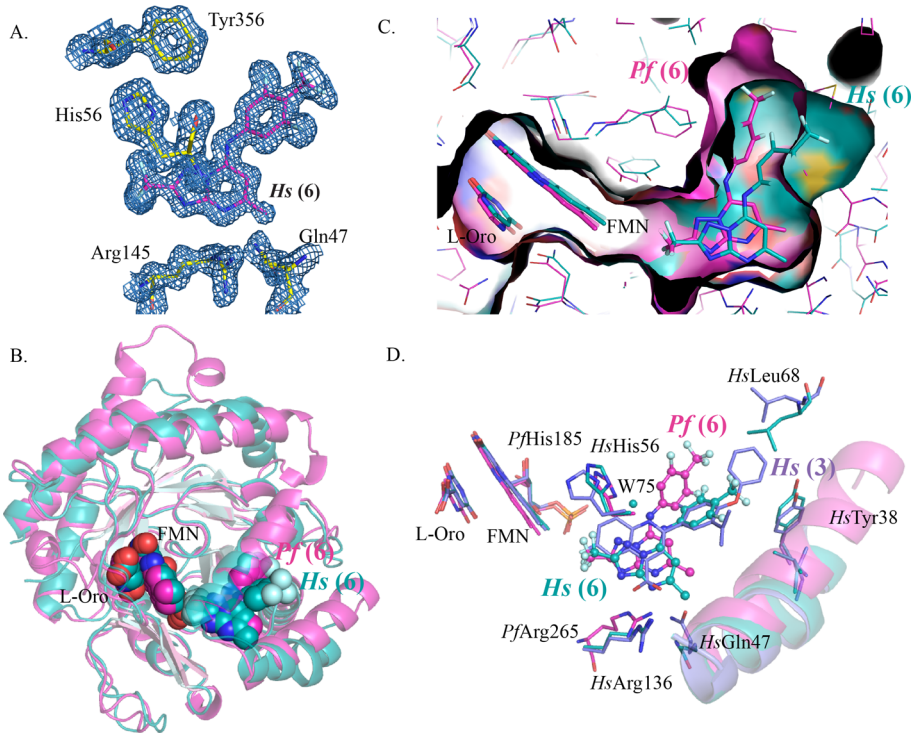

Figure 2. Crystal structures of *P. falciparum* DHODH and *Hs*DHODH bound to **6**. (A) $2F_o - F_c$ electron density map contoured at 1.0σ showing the **6** inhibitor binding site on *Hs*DHODH. The figure shows the map for the fully refined structure. (B) Ribbon diagram showing the alignment of the *Pf*DHODH–**6** (pink) structure with the *Hs*DHODH–**6** (turquoise) structure. (B, C) van der Waals surface representation of the aligned structures of *Pf*DHODH–**6** (pink) with *Hs*DHODH–**6** (turquoise). (D) Binding site alignment of *Pf*DHODH–**6** (pink), *Hs*DHODH–**6** (turquoise), and *Hs*DHODH bound to **3** (PDB 4IGH) (purple). A limited set of residues within the 4 Å shell are displayed.

enzymes, the improved binding from addition of the CF_2CH_3 or CF_3 to the C12 position on the triazolopyrimidine ring appears to combine additively with the effects of the *meta*-fluorines, leading to higher affinity on the rodent enzymes than to *Hs*DHODH.

X-ray Structure of 6 Bound to *P. falciparum*, Human, and Rat DHODH: Comparison of the Overall Binding Mode. To assess the structural underpinnings for the loss of species selectivity for analogues containing *meta*-fluorines on the aniline ring, we solved the X-ray structure of **6** bound to *P. falciparum*, human, and rat DHODH to 2.1, 1.2, and 1.5 Å, respectively (Supporting Information Table 1). Strong electron density for **6** was observed in the pockets of all three enzymes, allowing the binding modes of the inhibitor to be unambiguously determined (Figures 2A and Supporting Information Figure 1). *Pf*DHODH–**6** and *Hs*DHODH–**6** align with an rmsd of 1.8 Å, whereas the rat and human DHODH–**6** structures align closely with each other with an rmsd of 0.8 Å.

Compound **6** binds to *Pf*DHODH in the identical location and binding mode that was previously described for **8**[15] and **5**,[20] and no significant structural changes in the amino acid residues within 4 Å of the inhibitors were apparent (Figures 2B and Supporting Information Figures 2 and 3). The binding site is adjacent to the flavin mononucleotide (FMN) cofactor, with the triazolopyrimidine ring packed between helix α11 (residues 529–534) of the β/α-barrel domain and helix α2 (residues 181–189) (Figure 2B), which is part of the N-terminal extension that likely interacts with the mitochondrial membrane.

The triazolopyrimidine ring of **6** binds to human and rat DHODH in an overlapping site to that observed on *Pf*DHODH, although in the human and rat DHODH structures the triazolopyrimidine ring is tilted further toward helix α1 than it is in the *Pf*DHODH–**6** structure (Figures 2–4). **6** binds to human and rat DHODH in the same binding site as **2** and its analogues (e.g., **3**), with the binding orientation of **6** being nearly identical between the human and rat enzymes (Figures 2–4). In these structures, the 3,5-difluoro-4-trifluoromethyl aniline ring overlaps almost exactly with the central phenyl ring of **3** when bound to *Hs*DHODH (Figure 2D). The triazolopyrimidine ring overlaps with the quinolone ring of **3** but is shifted toward helix α1. H-bonds between the conserved Arg residue (R265 in *Pf*DHODH and R136 in human and rat DHODH) and the pyrimidine nitrogen N3 (Figures 5 and 6 and Supporting Information Table 2) are present in all three structures. The carboxylate group of **3** overlaps exactly with the pyrimidine nitrogen of **6** in the *Hs*DHODH and rat DHODH structures, suggesting that good interactions with the conserved Arg residue are a hallmark of high-affinity interactions with the inhibitor binding site.

In contrast to the triazolopyrimidine ring, the binding sites for the aniline ring are distinct between the *Pf*DHODH and human/rat DHODH structures (Figures 2D, 3, and 4A). As noted above, the aniline ring when bound to the mammalian enzymes accesses the same hydrophobic pocket that is utilized by **2** and **3**. The aniline ring of **6** is out of plane from the triazolopyrimidine ring in all three structures; however, the angle and direction of rotation from the plane differs between *Pf*DHODH and the human/rat structures. These differences lead to overall differences in the shape and orientation of the **6** binding site when bound to *Pf*DHODH versus the human enzyme (Figure 2C).

dx.doi.org/10.1021/jm500481t | *J. Med. Chem.* 2014, 57, 5381–5394

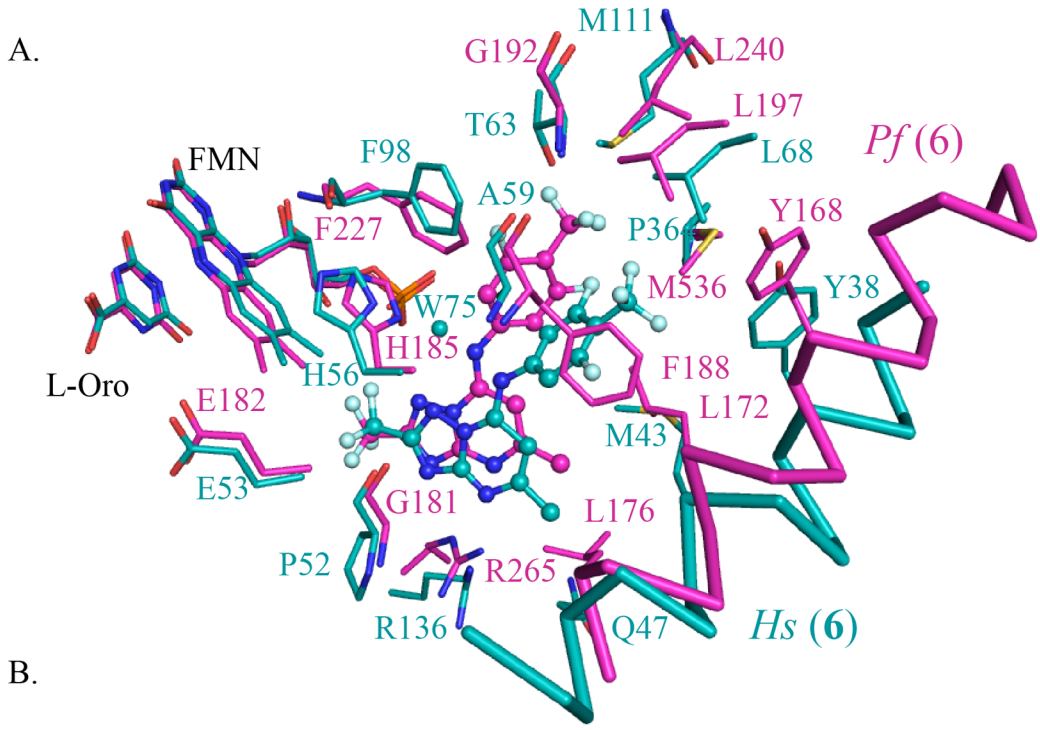

N-terminal

```
                        46        56      63   68
human           GDERFYAEHLMPTLQGLLDPESAHRLAVRFTSLGLLPRARFQDSDMLEVRVLGHKFRNPV 92
dog             GDEHFYAEHLMPAMQRLLDPESAHRLAVRVTSLGLLPRATFQESDMLEVRVLGHRFRNPI 110
rat             GDDHFYAEYLMPGLQRLLDPESAHRLAVRVTSLGLLPRATFQDSDMLEVKVLGHKFRNPV 92
mouse           GDDHFYAEYLMPALQRLLDPESAHRLAVRVISLGLLPRATFQDSNMLEVRVLGHKFRNPV 92
Pfalciparum     NPEFFLYDIFLKFCLKYIDGEICHDLFLLLGKYNILPYDTSNDSIYACTNIKHLDFINPF 221
                        175       185     192  197

                     98          111                       136
human           GIAAGFDKHGEAVDGLYKMGFGFVEIGSVTPKPQEGNPRPRVFRLPEDQAVINRYGFNSH 152
dog             GIAAGFDKHGEAVDGLYKMGFGFVEIGSVTPKPQEGNPRPRVFRLPEDQAVINRYGFNSH 170
rat             GIAAGFDKNGEAVDGLYKLGFGFVEVGSVTPQPQEGNPRPRVFRLPEDQAVINRYGFNSH 152
mouse           GIAAGFDKHGEAVDGLYKLGFGFVEVGSVTPQPQEGNPRPRVFRLPEDQAVINRYGFNSH 152
Pfalciparum     GVAAGFDKNGVCIDSILKLGFSFIEIGTITPRGQTGNAKPRIFRDVESRSIINSCGFNNM 281
                     227         240                       265
```

C-terminal

```
                     356 359  364
human           AGASLVQLYTALTFWGPPVVGKVKRELEALLKEQGFGGVTDAIGADHRR- 396
dog             AGASLVQLYTALTYRGPPVVGMIKRELEALLKEQGFTRITDAIGADHRR- 414
rat             AGASLVQLYTALIFLGPPVVVRVKRELEALLKERGFTTVTDAIGADHRR- 396
mouse           AGASLVQLYTALTFLGPPVVARVKRELEALLKERGFNTVTDAIGVDHRR- 396
Pfalciparum     AGASVCQLYSCLVFNGMKSAVQIKRELNHLLYQRGYYNLKEAIGRKHSKS 569
                     528 531  536
```

Figure 3. Structural and sequence alignments of *P. falciparum* and mammalian DHODH. (A) Inhibitor binding site showing the alignment of *Pf*DHODH−**6** (pink) and *Hs*DHODH−**6** (turquoise), with limited residues in the 4 Å shell displayed. (B) Sequence alignment of representative DHODHs. The full sequence alignment is shown in Supporting Information Figure 2.

Distinct *P. falciparum* and Mammalian DHODH Binding Modes for 6 Result from Amino Acid Differences in the Binding Pocket. The distinct binding modes of **6** when bound to *Pf*DHODH versus the mammalian enzymes are undoubtedly dictated by species differences in the amino acid composition of the aniline binding site (Figure 3 and Supporting Information Figure 2). The aniline site in the *Pf*DHODH structure is not present in the human structure because of the substitution of bulkier amino acids for the smaller residues observed in the *Pf*DHODH structure (e.g., *Hs*M111 for *Pf*L240 and *Hs*T63 for *Pf*G192). In addition, the position of *Hs*F98 relative to *Pf*F227 obstructs the *Pf*DHODH aniline binding mode as F98 in *Hs*DHODH is shifted toward the inhibitor pocket, protruding into the *Pf*DHODH aniline binding site. The position of F98 and the presence of T63 in the rat enzyme likewise occlude access to the *Pf*DHODH aniline pocket despite the observation that rat DHODH has a Leu at position 111, identical to the *Pf*DHODH residue (*Pf*L240) (Figures 3A, 4A, and 5B). However, this change apparently does not provide sufficient room in the pocket to

dx.doi.org/10.1021/jm500481t | *J. Med. Chem.* 2014, 57, 5381−5394

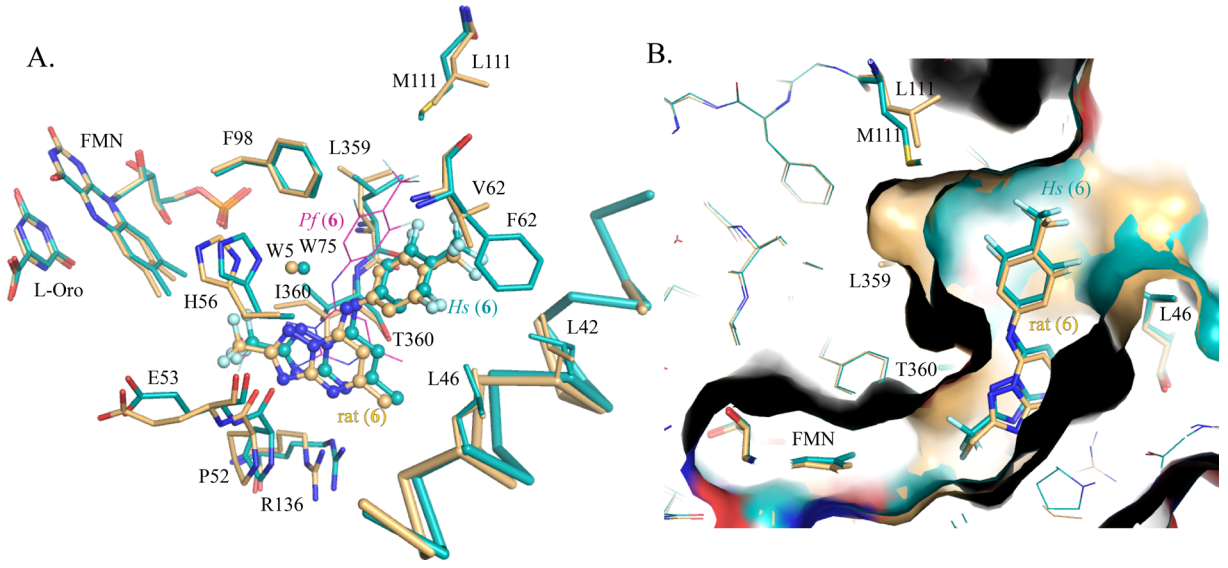

Figure 4. Alignment of the crystal structures of human and rat DHODH bound to **6**. (A) Alignment of *Hs*DHODH−**6** (turquoise) and rat DHODH (tan) showing the inhibitor binding site, with limited residues in the 4 Å shell displayed. **6** is shown as ball and stick. The position of **6** when bound to *Pf*DHODH is also shown superimposed and displayed by pink lines. (B) van der Waals surface representation of the aligned structures of *Hs*DHODH−**6** (turquoise) with rat DHODH (tan).

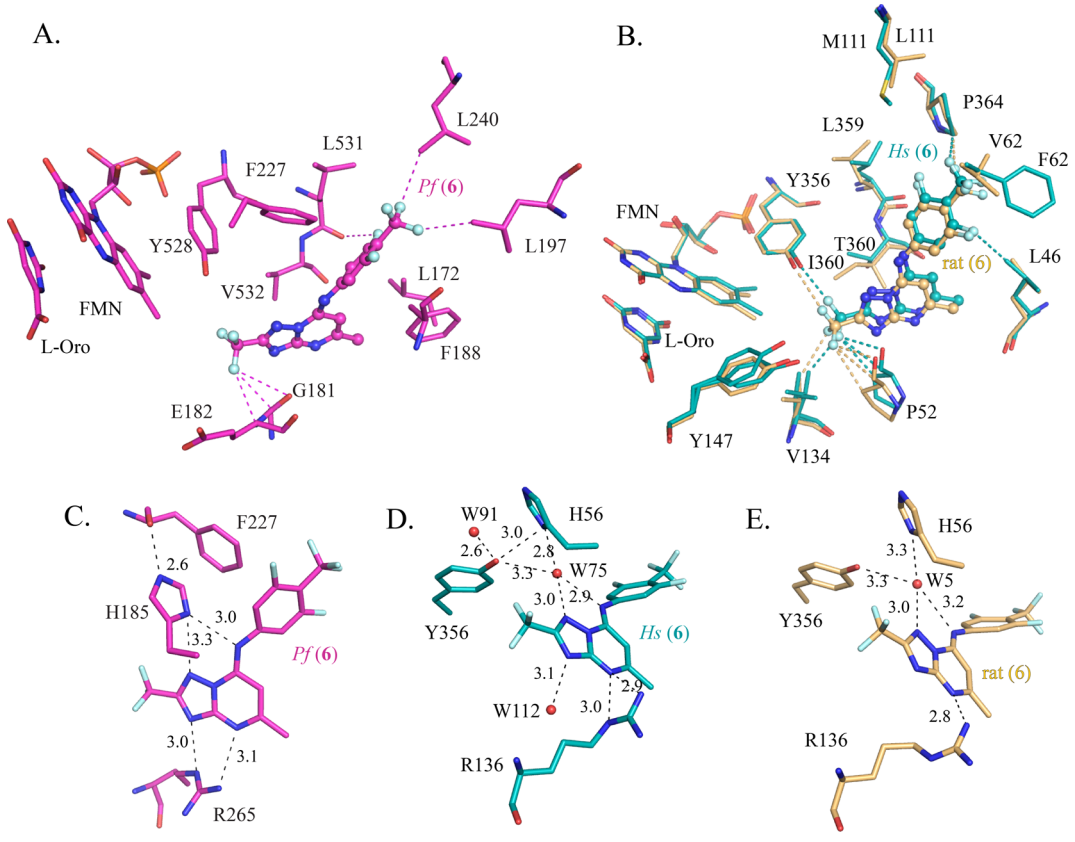

Figure 5. (A) *Pf*DHODH inhibitor binding site showing limited residues in the 4 Å shell. **6** is shown as ball and stick. Protein−fluorine contacts within 3.4 Å are indicated by dashed lines. (B) Alignment of *Hs*DHODH−**6** (turquoise) and rat DHODH (tan) showing the inhibitor binding site. (C) H-bond network between *Pf*DHODH and **6**. (D) H-bond network between *Hs*DHODH and **6**. (E) H-bond network between rat DHODH and **6**. H-bonds are indicated by black dashed lines, and distances are displayed in angstroms.

allow **6** to have access to the *Pf*DHODH aniline binding mode within the rat DHODH structure. On the flip side, the binding mode of the aniline ring on human and rat DHODH is inaccessible on *Pf*DHODH because of bulkier amino acid residues that occlude the pocket (e.g., *Pf*188 for *Hs*A59 and *Pf*M536 for *Hs*P364) (Figure 3).

The different binding modes on the malaria versus the mammalian enzymes lead to differences in many key interactions that have a demonstrated role in promoting

dx.doi.org/10.1021/jm500481t | J. Med. Chem. 2014, 57, 5381−5394

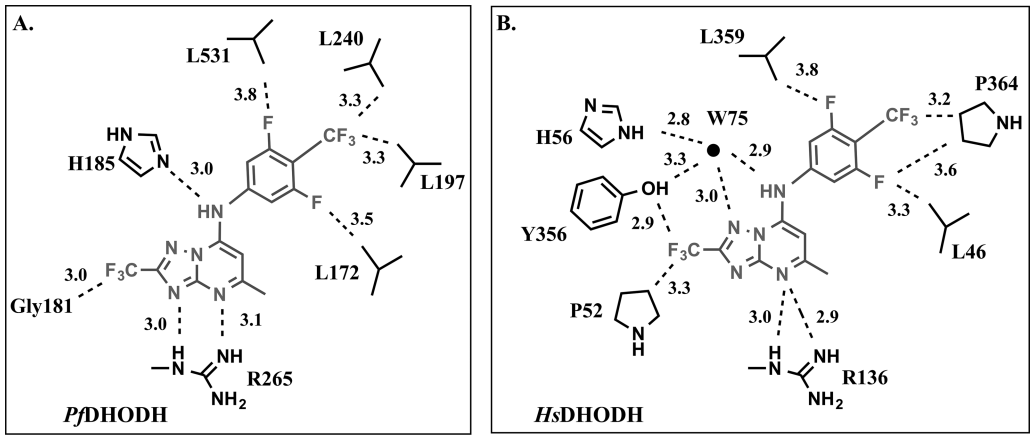

Figure 6. Schematic drawing of the (A) *Pf*DHODH and (B) *Hs*DHODH inhibitor binding sites. Inhibitor **6** is shown in gray, and protein side chains are shown in black labeled by amino acid and number. Select atom distances (in angstroms) are depicted by a dashed line.

binding to the malarial enzyme. In *Pf*DHODH, the aniline is involved in an edge-to-face stacking interactions with *Pf*F227 and *Pf*F188 (Figures 3A and 5A), and both residues have been shown to contribute to the binding affinity of triazolopyrimidine analogues by site-directed mutagenesis.[15] In contrast, in the human and rat structures, F188 is replaced by Ala (*Hs*A59), and the equivalent residue to F227 (*Hs*F98) is too far to form a stacking interaction with the aniline because of the shift of the binding site toward helix α1 (Figures 2D, 3A, and 4A). This shift has also changed the nature of the interaction with the anilide nitrogen (N1). In *Pf*DHODH−**6**, *Pf*H185 makes a direct H-bond interaction with N1 (Figures 3A and 5C), whereas in the human and rat structures, the equivalent residue, H56, forms an indirect interaction via a bridging water molecule (W75 in human and W5 in rat DHODH) (Figures 4A and 5D,E). W75/W5 also donates a H-bond to N5 of the inhibitor's triazolopyrimidine ring and has a close interaction (3.3A) with the hydroxyl of Tyr356. The *Hs*DHODH structure is the only structure of the three with a high enough resolution to show hydrogen atoms, and the data suggests that the ND1 of *Hs*H56 (nitrogen closest to **6**) and the N1 anilide nitrogen of **6** are both protonated and involved in the H-bond interaction with the bridging water (W75).

Binding Site Interactions between Compound 6 Fluorines and DHODH. The X-ray structures of *P. falciparum*, rat, and human DHODH bound to **6** show that the fluorinated groups make close contacts (<3.4 Å) with residues in all three binding sites (Figures 5A,B and 6 and Supporting Information Table 2). The most typical contacts are between fluorine and hydrocarbons, representing potential H-bonds with the aliphatic protons. Fluorines in the CF_3 group on the aniline ring make close contact (<3.4 Å) with the CD atom of P364 in the human and rat structures and with the CD1 atoms of *Pf*L197 and *Pf*L240 in the *Pf*DHODH structure. The *meta*-fluorines on the aniline ring are within 5 Å of two Leu residues in the inhibitor binding site, one positioned on either side of the aniline ring (Figure 5B and Supporting Information Table 2). *meta*-F7 is 3.3 and 3.7 Å, from CD1 of L46 in the human and rat DHODH−**6** structures, respectively, and several carbon atoms of L359 are within 4 to 5 Å of *meta*-F8 in the *Hs*DHODH and rat DHODH structures. Additionally, F8 in both structures is within 4 Å of the CD in P364 and within 4.3 Å of N in P364 (Figures 5B and 6 and Supporting Information Table 2). *meta*-Fluorine F8 is similarly near the equivalent residue on *Pf*DHODH (*Pf*L531) and makes a close contact with O of *Pf*L531 (3.3 Å) (Figure 5A and Supporting Information Table 2). The fluorines on the CF_3 at position C12 make the most extensive interactions in all three structures. In the human and rat enzymes, close contacts (<3.4 Å) are made between the CF_3 fluorines and the OH of Y356 the CG1 of V134 and between three atoms of P52 (O, CB, and C) (Figure 5B and Supporting Information Table 2). In the *Pf*DHODH structure, these contacts are replaced by interactions between NH of *Pf*E182 and with *Pf*G181 (O and C) (Figure 5A and Supporting Information Table 2).

Comparison of Rat and Human 6-Bound DHODH Structures. Although the addition of *meta*-fluorines increases binding affinity to all of the tested mammalian enzymes, binding to the rodent enzymes is significantly better than to the human and dog enzymes. Comparison of the rat and human DHODH−**6** structures shows that within the 5 Å inhibitor binding shell three amino acid residues differ between the two enzymes (rat: I360, L111, and V62 vs human: T360, M111, and F62) (Figures 4A and 5B). Position 360 forms extensive interactions with the triazolopyrimidine ring, and this residue is within 4.5 Å of the CF_3 group at C12. The different physiochemical properties of Ile versus Thr may contribute to the finding that addition of the CF_3 on C12 (**7** versus **8**) led to a significant increase in potency versus rat DHODH but not to *Hs*DHODH (Table 1). The smaller residue at position 111 in rat DHODH makes the overall binding pocket larger than in the human enzyme, as does the shift of L359 away from **6** (Figure 4B). The CB carbons of F62 and L62 are within 4.1 Å of the aniline CF_3 groups, but the F62 ring is too far to form an edge-to-face stacking interaction with the aniline ring of **6** and there are no direct interactions with the side chains of these residues that would suggest an impact on binding.

Small Molecule X-ray Structures of 6 and 7. In our previous work, small molecule X-ray crystallography of triazolopyrimidines from the series (notably, DSM1, which has a naphthlene in place of the aniline ring) showed partial double-bond character between N1 and C8 (the observed bond length was 1.31 Å),[15] suggesting delocalization of electrons onto N3, whereas the N1−C8 distance (1.344 Å) for the weaker binding **8** showed no double-bond character. To evaluate the effects of *meta*-fluorines on bond distances, we solved the small molecule X-ray structures of **6** and **7** (Table 2, Supporting Information Table 3, and Supporting Information

dx.doi.org/10.1021/jm500481t | J. Med. Chem. 2014, 57, 5381−5394

Table 2. Selected Bond Distances from Small Molecule X-ray Crystallography[a]

inhibitor	6	7	8
C1−N1	1.393(6)	1.423(6)	1.42(2)
	1.415(6)	1.432(6)	
		1.419(6)	
C8−N1	1.362(6)	1.341(6)	1.344(4)
	1.364(6)	1.338(6)	
		1.345(6)	

[a]Data are shown for all molecules in the asymmetric unit. Typical sp^2 C−N and C=N bond lengths are usually 1.38 and 1.28 Å, respectively.[44] Data for **8** were previously reported.[15]

Figure 4). The N1−C8 bond distances for **6** and **7** were consistent with single C−N bond lengths, although there was a tendency for the bond length to increase with the addition of *meta*-fluorines, particularly for **6** (Table 2). Concomitantly, there was a trend toward a shortening of the N1−C1 bond length in **6**, consistent with the electron-withdrawing effects of two *meta*-fluorines on the aniline ring. The anilide nitrogen (N1) was protonated in both structures, whereas the pyrimidine nitrogen (N3) was not (Supporting Information Figure 4). The pK_a's of N1 were calculated for the series, showing that each *meta*-fluorine is predicted to lower the pK_a by approximately 0.8−1 pK_a units (Table 1). These data suggest that the electron-withdrawing effects of the *meta*-fluorines on the aniline ring influence the properties of the anilide nitrogen (N1).

Thermodynamic Analysis of Inhibitor Binding to *P. falciparum* and Rat DHODH. In order to better understand the nature of the binding affinity for the best triazolopyrimidine analogues against *Pf*DHODH, we collected isothermal titration calorimetry (ITC) data for a matched set of analogues to test the affects of both C12 substitution and addition of *meta*-fluorines to the aniline ring on the equilibrium dissociation constant (K_d) and on the thermodynamic parameters (ΔH and ΔS) (Table 3 and Supporting Information Figure 5). Analysis of the thermodynamic parameters showed that, with the exception of **8**, all analogues demonstrated a favorable contribution of both enthalpy and entropy to the *Pf*DHODH binding interaction, although the enthalpic term was larger in all cases. The contribution of enthalpy to binding was most pronounced for **8**, which was the only compound to show an unfavorable entropic term. In this assay, addition of fluorocarbons at C12 on the triazolopyrimidine ring led to a 10-fold improvement in binding affinity, whereas the addition of *meta*-fluorines led to a 3−5-fold improvement. The better binding affinity of analogues containing fluorocarbons at the C12 position is entropically (ΔS) driven, suggesting that the increased binding affinity results from hydrophobic interactions. The increased contribution of the entropic term to binding in the series parallels compound hydrophobicity (Table 3, LogD values). Similarly, the binding impact of *meta*-fluorines was manifest in ΔS. The ITC-derived *Pf*DHODH K_d correlates with both the parasite IC_{50} and the kinetically derived *Pf*DHODH IC_{50}, although, with the exception of **5**, the ITC-derived K_d value is a better predictor of antiparasite activity than the kinetically derived IC_{50}. The kinetically derived IC_{50} values may be complicated by tight binding kinetics, suggesting that ITC provides a more representative measure of the inhibitor binding affinity for compounds with binding constants in the low nanomolar range.

ITC data were also collected for rat DHODH, although solubility limitations combined with weaker or undetectable binding prevented a full set of data for the tested analogues on the mammalian enzymes from being obtained. We were able to obtain ITC data for **6** and **11** binding to rat DHODH. For **11**, the measured K_d was in good agreement with the kinetically derived IC_{50} (Tables 1 and 3), but for **6**, the sharpness of the transition prevented determination of K_d and ΔS, so only ΔH is reported. In contrast to the binding interactions with *Pf*DHODH, the interaction of **11** with rat DHODH was dominated by the entropic term, suggesting that hydrophobic interactions dominate binding to the mammalian enzymes (Table 3). Although ΔS could not be calculated for **6**, ΔH is similar to that observed for **11**, and given their similar binding affinity in the kinetically derived assay, these data suggest that binding of **6** will also be dominated by the entropic term.

Evaluation of *Hs*DHODH Ligand Interactions by Site-Directed Mutagenesis. To evaluate the energetic contribution of key amino acid residues in the **6** binding site, we performed site-directed mutagenesis. We selected residues within the H-bond network (*Hs*H56 and *Hs*R136) and two hydrophobic residues that were near the *meta*-fluorines (*Hs*L46 and *Hs*L359) (Figure 5 and Supporting Information Table 2) for analysis. All four residues were replaced with Ala in *Hs*DHODH, and the effects on the steady-state kinetic parameters (K_m and k_{cat}) and on inhibitor binding affinity (Tables 4 and Supporting Information Table 3) were characterized. The steady-state kinetic constants (K_m and k_{cat}) were within 10-fold of wild-type values for all four mutants (Supporting Information Table 3). Background oxygen-dependent activity for the *Hs*DHODH L46A, L359A, and R136A mutants (CoQ-independent activity) was similar to wild-type *Hs*DHODH, accounting for ∼10% of k_{cat}. In contrast, *Hs*H56A showed almost no CoQ-dependent activity in the 2,6-dichloroindophenol (DCIP)-based assay. *Hs*H56A activity was,

Table 3. Thermodynamic Study of DHODH−Inhibitor Interactions[a]

		*Pf*DHODH			rat DHODH		
inhibitor	LogD	K_d μM (1σ)	ΔH kcal/mol	$-T\Delta S$ kcal/mol	K_d μM (1σ)	ΔH kcal/mol	$-T\Delta S$ kcal/mol
8	3.55	0.17 (0.11−0.26)	−10 (−12 to −9.8)	1.5	nd	nd	nd
5	4.05	0.027 (0.010−0.063)	−8.3 (−9.2 to −7.5)	−2.2	nd	nd	nd
10	4.25	0.0098 (0.0061−0.015)	−9.0 (−9.3 to −8.7)	−2.1	nd	nd	nd
11	4.46	0.0051 (0.0015−0.016)	−8.1 (−8.8 to −7.5)	−3.3	0.048 (0.0084−0.143)	−2.1 (−2.5 to −1.9)	−8.0
6	5.01	0.0096 (0.0040−0.019)	−6.5 (−6.9 to −6.2)	−4.5	CNC	−1.6 (−1.8 to −1.5)	CNC

[a]Studies were performed at 303 K. The 1σ confidence interval is displayed in parentheses for three independent experiments. The *Pf*$DHODH_{\Delta 384-413}$ expression construct was used for the study. ND, not determined. CNC, could not calculate because the sharpness of the transition prevented an accurate determination of these values. For the free energy of binding, $\Delta G = \Delta H - T\Delta S$.

dx.doi.org/10.1021/jm500481t | J. Med. Chem. 2014, 57, 5381−5394

Table 4. Kinetic Analysis of Inhibitor Binding to Human Wild-Type and Mutant DHODHs[a]

	IC_{50} (uM)				
enzyme	1	5	10	11	6
WT 33−396	0.21 (0.16−0.26)	>100	45 (36−54)	2.7 (1.8−3.9)	2.1 (1.5−3.1)
L46A	0.27 (0.17−0.43)	>100	>100	>100	>100
H56A	1.5 (0.8−3.0)	>100	67 (31−100)	5.3 (2.5−10.9)	0.9 (0.7−1.1)
R136A	36 (24−48)	>100	>100	>100	>100
L359A	0.28 (0.22−0.36)	>100	>100	>100	35 (23−47)

[a]The *Hs*DHODH$_{33-396}$ construct was used for the mutant analysis. The 95% confidence interval is displayed in parentheses. The data set included three replicates for each inhibitor concentration used in the fit. Experiments were conducted using the direct assay.

therefore, evaluated using the direct assay in the presence of an oxygen depletion system, demonstrating that the CoQ-dependent k_{cat} was decreased by 4-fold in comparison to the that of wild-type enzyme. The direct assay was then used to evaluate the inhibitor binding kinetics for all of the mutants (Table 4). The *Hs*R136A, *Hs*L46A, and *Hs*L359A mutations led to reduced binding of the tested triazolopyrimidine inhibitors, whereas *Hs*H56A was inhibited to the same extent as that of the wild-type enzyme. For the tightest binding inhibitors, **6** and **11**, the *Hs*R136A and *Hs*L46A mutations led to a 50-fold reduction in binding affinity, whereas the *Hs*L359A mutations lead to >50- and 10-fold reductions, respectively (Table 4). Both *Hs*H56 and *Hs*R136 were important binding determinants for **1**, where mutation led to 7- and 100-fold increases in IC_{50}, respectively. In contrast, for **1** the *Hs*L46A and *Hs*L359A mutant enzymes showed similar binding affinity as that to the wild-type enzymes. Both *Hs*R136 and *Hs*H56 are within 3.5 Å of A77 1726 in the reported X-ray structure (PDB 1D3H).[17] L46 is outside the van der Waals shell (>4 Å), whereas *Hs*L359 CG does form a contact with fluorine on the CF_3 group (distance 3.3 Å), but, apparently, it is not a key contributor to the binding affinity.

DISCUSSION

The triazolopyrimidine scaffold has proved to be a highly successful chemical class for the identification of potent and species-selective *Pf*DHODH inhibitors, leading to the discovery of a clinical development candidate.[20] Optimization of the series relied on the introduction of fluorocarbons to improve both metabolic stability and potency. Herein, we explored the effects of combining *meta*-fluorine substitutions on the aniline ring with the addition of fluorocarbons on C12 of the triazolopyrimidine ring. In this context, the addition of the *meta*-fluorines led to modestly increased binding affinity toward *Pf*DHODH, but surprisingly, these modifications also led to binding of these analogues to mammalian DHODHs, with the rank order of potency being rat > mouse > dog ≫ human DHODH. Although these compounds still retained strong selectivity toward *Pf*DHODH versus *Hs*DHODH, the selectivity window was decreased from >2500-fold to only 100-fold for compounds with two *meta*-fluorines, and selectivity was lost altogether versus the rodent enzymes. Thus, despite their intrinsic potency, compounds containing the combination of *meta*-fluorines on the aniline with fluorocarbons at C12 of the triazolopyrimidine ring will not be useful development candidates for malaria. The reduced window of selectivity on *Hs*DHODH is the largest factor, but additionally, the lack of selectivity versus rodent DHODH would prevent mouse or rat from serving as good toxicologic models to predict safety in humans. Interestingly, the potency of the most heavily fluorinated compounds toward *Hs*DHODH was within 10-fold of **1**, the active metabolite of leflunomide, which is used clinically for the treatment of arthritis and multiple sclerosis. These data suggest that compounds with potential for use as immune suppressive agents in humans could be identified from the triazolopyrimidine scaffold, although **6** in particular has certain pharmacological properties that are atypical of the series and that suggest it should not be advanced further in the drug development pipeline.

We previously speculated that the strong species selectivity of triazolopyrimidine compounds resulted from differences in the amino acid composition of the inhibitor binding site between human and *P. falciparum* DHODH,[15] and indeed, the current study confirms that the binding mode for these inhibitors on *Pf*DHODH is not accessible on the mammalian DHODH structures because of these amino acid changes. However, the current study also demonstrates that an alternative binding mode is available on the human and rat enzymes, and although **8** and other analogues that lack extensive fluorination do not bind the mammalian enzymes, it is not because steric constraints prevent binding but instead because the available binding site on the mammalian enzymes is inherently a lower-affinity site. The triazolopyrimidine inhibitor binding site in both *P. falciparum* and mammalian DHODHs is primarily hydrophobic with only two possible H-bonding interactions between the protein and inhibitor. The inhibitor−protein interaction involving the conserved Arg (*Pf*R265/*Hs*R136/*r*R136) is similar in all three structures, and the energetic consequence of mutating *Hs*R136 to Ala in *Hs*DHODH (50-fold decrease in binding affinity) was similar to the consequence of the *Pf*R265A mutation on binding **8** and related analogues.[15] In contrast, the nature of the interaction with the conserved His (*Pf*H185/*Hs*H56/*r*H56) is very different between the parasite and mammalian DHODHs. In *Pf*DHODH, a direct H-bond is formed between aniline NH (N1) and the H185 imidazole ND1, whereas in the human and rat enzymes, the interaction with H56 is mediated by an ordered water. Imidazole is a better Lewis base and H-bond acceptor than water, suggesting that the H-bond with H185 in *Pf*DHODH provides significantly more binding energy than the interaction between **6** and the water molecule in the mammalian enzymes. Moreover, in mammalian DHODH, this water forms a number of other H-bonds with nearby groups, and the final orientation of water will be a compromise to minimize the local free energy across all water/nearest neighbor interactions. The inability of the triazolopyrimidine compounds to form a direct H-bond with the invariant His residue in the mammalian enzymes is thus likely to be one of the primary contributors to species selectivity, except in the case of analogues containing extreme fluorination (discussed below). The substantially higher contribution of the enthalpic term for binding of **6** and **11** to *Pf*DHODH in comparison to rat

dx.doi.org/10.1021/jm500481t | J. Med. Chem. 2014, 57, 5381−5394

DHODH supports this conclusion, as does the finding that mutation of H185 in *Pf*DHODH leads to a substantial loss in inhibitor binding affinity (25−100-fold).[15] In contrast, although the interaction with the binding site water cannot be probed directly, mutagenesis of H56, which coordinates the water, in *Hs*DHODH did not have a significant impact on binding.

As discussed, most triazolopyrimidine inhibitors have little or no activity against mammalian DHODHs, but increasing fluorine substitution dramatically increased binding to mammalian DHODHs. Several factors likely contribute to the enhanced binding of these analogues to the mammalian enzymes, including potentially specific fluorine−protein interactions and the overall hydrophobic effects of fluorination. Many structures of proteins bound to ligands containing fluorines are present in the PDB database, providing an index of the type of contacts that are observed between the fluorine ligands and proteins.[25,26] The most common fluorine interactions occur with sulfur, hydroxyl, or guanidinium; however, few studies experimentally test how these interactions contribute to binding energy. Quantum mechanical calculations suggest that fluorine acts as an H-bond acceptor because fluorine retains a partial negative charge.[25,26] The X-ray structures of **6** bound to mammalian and *Pf*DHODH demonstrate that few contacts between fluorines and protein are within 3.3 Å, and we observed no contacts with sulfur or guanidinium. A few close electrostatic contacts (<3.3 Å) that could contribute positive binding interactions include Y356 OH with F4 in the human and rat structures and an interaction between F5 and a NH (E182) in the *Pf*DHODH−**6** structure. However, the majority of the close contacts occur with methyl groups on aliphatic side chains. The existence of weak H-bonds between fluorine and hydrogen participating in CH bonds has been observed in small molecule complexes,[27,28] suggesting that these interactions could contribute to binding energy. Finally, the electron-withdrawing effects of the *meta*-fluorines are predicted to lower the pK_a of the aniline nitrogen (N1), which would improve the H-bond capability of N1. The small molecule X-ray crystallography showed a shortening of the C1−N1 bond distance in **6**, consistent with the expected electron-withdrawing effect of the *meta*-fluorines. However, improved H-bonding with the ordered water molecule in the human and rat enzymes is unlikely to be the main factor in the improved binding to the mammalian enzymes because the enthalpic contribution to binding of **6** and **11** to the rat enzyme is small.

The addition of fluorine to a ligand is known to increase hydrophobicity, and indeed, the LogD of compounds in the triazolopyrimidine series increased, as expected, with increasing fluorination. The fact that the inhibitor binding pocket is largely hyrdrophobic in the *Plasmodium* and mammalian DHODHs suggest that the increased fluorination may impact binding affinity through the hydrophobic effect. Quite notably, the rat and human enzymes position Leu residues (L46 and L359) on opposite sides of the *meta*-fluorines on the aniline ring. These Leu residues may provide a particularly supportive hydrophobic environment for binding analogues with *meta*-fluorines over those that do not have this substitution. Our site-directed mutagenesis studies on the human enzyme support a role for L46 and L359 in enhancing binding to the human enzyme. Within the inhibitor series, binding to *P. falciparum* DHODH shows both a positive enthalpic and entropic contribution, and although the enthalpic contribution is larger in all cases, the addition of fluorocarbons to C12 increases the contribution to binding of the entropic term, as does addition of *meta*-fluorines. Indeed, synthesis of these analogues was predicated on the hypothesis that the strongly electronegative characteristics of the fluorine atoms would reduce the Lewis basicity of neighboring nitrogens in the triazolopyrimidine core, thus reducing the desolvation penalty and giving an entropic benefit to the potency. In comparing binding to the *P. falciparum* and rat enzymes, notably, **11** binds both enzymes with similar affinity. Enthalpy contributes more to binding to *Pf*DHODH than entropy, whereas the entropic term is very significantly the dominant factor for binding to rat DHODH. These data suggest that hydrophobic interactions dominate the interaction between rat DHODH and **11** and support the hypothesis that the addition of *meta*-fluorines to the scaffold improves binding to the mammalian enzymes through hydrophobic interactions. Although some studies have suggested that binding interactions between fluorine and lipophilic pockets are weak,[25,26] studies on fluorinated coiled−coiled dimers have shown that peptides with mixed hydrocarbon−fluorocarbon cores are highly stable, providing evidence for good packing interactions between fluorocarbons and alkyl carbons.[29] Fluoracetyl-CoA specific thioesterase shows stringent specificity for the fluorinated substrate over acetyl-CoA by 10^6-fold, and this selectivity has been attributed in part to be a result of greater chemical reactivity. However, binding the fluorinated substrate into a hydrophobic pocket was also speculated to be enhanced because of the entropic advantage of releasing bound water molecules.[30] A similar effect on solvent could also be at play with our triazolopyrimidine analogues.

Addition of the *meta*-fluorines resulted in a modest 2−4-fold improved binding affinity of **6** to *Pf*DHODH but up to 100-fold increase in binding affinity to the human and rat enzymes. It is possible that the smaller effect on *Pf*DHODH is due to the net effect of two opposing effects of fluorine on inhibitor binding. One notable difference between *Pf*DHODH and the mammalian enzymes is the presence of edge-to-face stacking interactions between the aniline ring and *Pf*DHODH active site residues (F227 and F188), which were previously shown to be important for high-affinity binding.[15] These stacking interactions are absent in the mammalian enzymes because the F227 equivalent residue (F98) is too far from the inhibitor to form an interaction and because F188 is replaced with Ala. Thus, these interactions also differentiate the binding modes between the parasite and mammalian enzyme and are also likely to contribute to selectivity. Fluorination of an aromatic ring is thought to lead to weakening of aromatic stacking interactions.[25,26] Thus, potentially weakening of the edge-to-face stacking interactions in *Pf*DHODH occurs upon addition of the *meta*-fluorines to the aniline ring, offsetting any other positive impact of the increased hydrophobicity on binding. Additionally, the data may suggest that the overall binding pocket on the mammalian enzymes is more hydrophobic than the pocket on *Pf*DHODH, leading to greater enhancements in binding as the LogD increases with increased fluorination of the aniline ring.

Finally, although the effects on inhibitor binding because of the *meta*-fluorines appear to be similar on the rat and human enzymes, CF_3 or CF_2CH_3 groups at C12 enhanced binding affinity toward *P. falciparum*, rat, and mouse DHODH (by 5−25-fold) but did not result in measurable binding interactions with the human enzyme. Three amino acid differences between human and rat DHODH (M111 vs L111; F62 vs V62; and T360 vs I360) within the inhibitor binding site may provide

insight into the weaker binding of these analogues to the human enzyme. The more hydrophilic nature of T360 on *Hs*DHODH versus I360 on rat DHODH may contribute to weakening the hydrophobic effect on binding of the inhibitors. Mouse DHODH also contains a Thr at position 360 (Figure 3B), but addition of fluorocarbons to C12 had similar effects on binding of the analogues to the mouse enzyme as to the rat enzyme. However, in the case of the mouse enzyme, the additional substitution of Thr63 with Ile in the inhibitor pocket may offset the effects of the hydrophilic residue at position 360.

CONCLUSIONS

We have demonstrated that the addition of fluorines into the triazolopyrimidine class of *Pf*DHODH inhibitors can have a profound effect on binding affinity and species selectivity. Our studies importantly define the requirements for species-selective binding to malaria DHODH and teach us how to maintain wide safety windows when optimizing DHODH inhibitors for antimalarial activity. Our data show that a primary factor in species selectivity is the ability of these inhibitors to form a direct H-bond between the conserved active site His (*Pf*H185) on *Pf*DHODH that is not formed on the mammalian enzymes. As a consequence, the enthalpic contribution of binding to the mammalian enzymes is lower than for binding to *Pf*DHODH. The improved binding of heavily fluorine-substituted triazolopyrimidines to the mammalian DHODHs seems to be a consequence of an enhanced hydrophobic effect owing to increasingly hydrophobic inhibitors binding in a primarily apolar binding site. Two key Leu residues positioned on either side of the *meta*-fluorines contribute to binding, and several likely H-bonds between fluorine and aliphatic protons were also observed. Our data provide compelling evidence that fluorine can enhance binding to lipophilic pockets, and they suggest that packing of fluorocarbons with alkyl side chains in proteins is energetically favorable. Compounds with both *meta*-fluorines on the aniline ring and fluorocarbons at C12 of the triazoloprymidine ring have poor species selectivity and thus will not be useful as development candidates against malaria. However, these studies show for the first time that the triazolopyrimidine scaffold can be engineered to identify potent inhibitors of human DHODH, a finding that has the potential to impact drug discovery for the treatment of rheumatoid arthritis, multiple sclerosis, and other autoimmune diseases.

METHODS

Chemical Synthesis. The syntheses of **8** ((5-methyl[1,2,4]-triazolo[1,5-*a*]pyrimidin-7-yl)(4-trifluoromethylphenyl)amine), **9** (*N*-(3,5-difluoro-4-(trifluoromethyl)phenyl)-5-methyl-[1,2,4]triazolo[1,5-*a*]pyrimidin-7-amine), **7** (2-(trifluoromethyl)-*N*-(4-(trifluoromethyl)-phenyl)-5-methyl-[1,2,4]triazolo[1,5-*a*]pyrimidin-7-amine), and **5** (2-(1,1-difluoroethyl)-5-methyl-*N*-[4-(trifluoromethyl)phenyl]-[1,2,4]-triazolo[1,5-*a*]pyrimidin-7-amine) were previously reported.[20−22] Synthesis of the remaining triazolopyrimidines, **6**, **10**, and **11**, was accomplished using the same methods. All compounds were determined to be >95% pure by LCMS. Experimental data for these compounds are as follows:

6 (*N*-(3,5-difluoro-4-(trifluoromethyl)phenyl)-2-(trifluoromethyl)-5-methyl-[1,2,4]-triazolo[1,5-*a*]pyrimidin-7-amine).[31] mp 86−88 °C. ^{1}H NMR (300 MHz, $CDCl_3$): δ 8.29 (brs, NH, exchangeable), 7.14 (d, J = 9.7 Hz, 2H), 6.77 (s, 1H), 2.70 (s, 3H). MS m/z 398.2 $[M + H]^+$.

10 2-(1,1-difluoroethyl)-*N*-[3-fluoro-4-(trifluoromethyl)phenyl]-5-methyl [1,2,4]triazolo[1,5-*a*]pyrimidin-7-amine.[31] ^{1}H NMR (400 MHz, DMSO-d_6): δ 10.69 (bs, 1H), 7.84 (m, 1H), 7.63−7.45 (m, 2H), 6.91 (s, 1H), 2.50−2.48* (pr, 3H), 2.13 (t, J = 19.2 Hz, 3H). ES+ MS m/z 376 $(MH)^+$. *Note that this spectrum was obtained using deuterated DMSO and that the signal from the methyl group overlaps the signal from the residual DMSO (at 2.5 ppm), so both signals are reported.

11 (*N*-(3,5-difluoro-4-(trifluoromethyl)phenyl)-2-(1,1-difluoroethyl)-5-methyl[1,2,4]-triazolo-[1,5-*a*]pyrimidin-7-amine).[31] mp 80−82 °C. ^{1}H NMR (500 MHz, $CDCl_3$): δ 8.08 (brs, NH, exchangeable), 7.09 (d, J = 9.17 Hz, 2H), 6.75 (s, 1H), 2.72 (s, 3H), 2.20 (t, J = 18.70 Hz, 3H). MS m/z 394.3 $[M + H]^+$.

Gene IDs. The following DHODH (EC 1.3.5.2) proteins were used in this study, and their GeneBank or PlasmoDB accession numbers are shown in parentheses. *Pf*DHODH, PlasmoDB (PF3D7_0603300), *Hs*DHODH (NP_001352.2), rat DHODH (NP_001008553.1), mouse DHODH (NP_064430.1), and dog DHODH (XP_853399.2).

DHODH *Escherichia coli* Expression Plasmids Used for IC_{50} Determination. DHODHs were expressed as truncated, soluble enzymes where the N-terminal mitochondrial membrane domains had been removed. Expression plasmids for N-terminally His_6-tagged *Pf*DHODH residues 158−569 (pRSETb-*Pf*DHODH$_{158-569}$) and C-terminally His_6-tagged *Hs*DHODH (pET-22b-*Hs*DHODH$_{30-396}$ with N-terminal sequence 30-MATGDE) were previously described.[32,33] *E. coli* codon-optimized genes encoding the mouse, rat, and dog DHODH enzymes were synthesized by GenScript and cloned into the pET-28b vector (Novagen) at the NcoI and XhoI sites to generate the C-terminal His_6-tag fusion proteins. The final expression vectors are as follows: mouse DHODH (pET-28b-*Mouse*DHODH$_{30-396}$; N-terminal sequence 30-*MA*TATGDD); rat DHODH (pET-28b-*rat*DHODH$_{30-396}$; N-terminal sequence 30-*MA*TATGDD) and dog DHODH (pET-28b-*dog*DHODH$_{48-414}$; N-terminal sequence 48-*MA*TAMGDE), where the underlined sequence represents the DHODH gene specific sequence, and the amino acids in italics represent vector-derived sequence to allow the protein to be in frame with the start Met. For mammalian DHODH, numbering is based on the reported X-ray structures.[17]

DHODH *E. coli* Expression Plasmids Used for X-ray Crystallography and ITC Analysis. Expression constructs for crystallization of *Pf*DHODH (pET28b-*Pf*DHODH$_{\Delta 384-413}$; N-terminal His_6-tag_TEV protease site, *Pf*DHODH residues 158−569 with a Δ384−413 deletion) and human DHODH (pET28b-*Hs*DHODH$_{33-396}$; C-terminal His_6-tag) were previously described.[14,34] The additional truncations relative to constructs used for IC_{50} determination were found to improve crystal diffraction while not affecting enzyme activity (k_{cat} and K_m). Two expression plasmids for rat DHODH were tested in crystallographic studies. The cloning of the first pET28b-ratDHODH$_{30-396}$ was described above. This clone was then used as the template for deletion mutagenesis using the QuikChange kit (Strategene) as recommended by the manufacturer to generate pET28-ratDHODH$_{33-396}$ using the following primers: GAAGGAGATATACCATGGGTGACGACCACTTCTATGC and GCATAGAAGTGGTCGTCACCCATGGTATATCTCCTTC. The latter smaller construct was found to produce better quality crystals and was used to generate the protein for solution of the rat DHODH−**6** structure described below.

Purification of DHODH from *E. coli*. Recombinant enzymes were expressed in BL21 phage-resistant *E. coli* (Novagen) and purified by Ni^{2+} affinity column chromatography as previously described.[15,34] In the final step, protein was fractionated on a HiLoad 16/60 Superdex 200 column (GE Healthcare) equilibrated with buffer (10 mM Hepes, pH 7.8, 300 mM NaCl, 5% Glycerol, 10 mM dithiothreitol (DTT)) plus detergent. Triton (0.05%) was added for enzymes purified for IC_{50} determination, and the following detergents were used for crystallizations: 1 mM *N*,*N*-dimethyldodecylamine *N*-oxide (LDAO, Fluka) for *Pf*DHODH, 80 mM HEGA-9 (Anatrace) for rat DHODH, and a combination of 40 mM Zwittergent 3-10 (Affymetrix) and 200 mM HEGA-8 (Affymetrix) for human DHODH. Protein concentration was determined by following absorbance at 280 nm using the following extinction coefficients: rat, mouse, and dog DHODH, 11.92

dx.doi.org/10.1021/jm500481t | J. Med. Chem. 2014, 57, 5381−5394

cm^{-1} mM^{-1}; *Pf*DHODH, 29.1 cm^{-1} mM^{-1}; and *Hs*DHODH, 15.93 cm^{-1} mM^{-1}.

Site-Directed Mutagenesis. *Hs*DHODH mutant enzymes were created in the pET28b-*Hs*$DHODH_{33-396}$ expression construct by site-directed mutagenesis using the QuikChange kit (Strategene) as recommended by the manufacturer. pET28b-*Hs*$DHODH_{33-396}$ (25 ng) was used as template, and 100 ng of each primer was used for each reaction. Annealing temperature was set over a linear range (60−65 °C), and the extension temperature was at 72 °C. Primers used for the mutagenesis were as follows: L46A (primers: CTGATGCCGACT-GCGCAGGGGCTGCTG and CAGCAGCCCCTGCGCAGTCG-GCATCAG), L359A (primers: GCAGCTGTACACGGCCGCCAC-CTTCTGG and CAGAAGGTGGCGGCCGTGTACAGCTGC), R136A (primers: GACCCAGAGTCTTCGCCCTCCCTGAGGAC and GTCCTCAGGGAGGGCGAAGACTCTGGGTC), and H56A (primers: CCGGAGTCAGCCGCCAGACTGGCTGTTC and GAACAGCCAGTCTGGCGGCTGACTCCGG).

Crystallization. Crystallizations were performed by the hanging-drop vapor-diffusion method at 20 °C. Preliminary crystallization conditions were found using the random crystallization screen AmSO4 and Cryo suites (NeXtal), and conditions were then refined by varying the pH, precipitant, and protein concentration. Crystals of the *Pf*$DHODH_{\Delta384-413}$**−6** complex were obtained by mixing reservoir solution (0.16 M ammonium sulfate, 12−13% PEG4000, 0.1 M sodium acetate, pH 4.8, and 10 mM DTT) with an equal volume of *Pf*$DHODH_{\Delta384-413}$ (33 mg/mL) pre-equilibrated with 2 mM **6** (in DMSO solution) and 2 mM dihydroorotate (DHO). Crystals of *Hs*$DHODH_{33-396}$**−6** were obtained by mixing reservoir solution (1.76 M ammonium sulfate, 0.1 M Sodium acetate, pH 5.4, 1.9 M NaCl, and 10 mM DTT) with an equal volume of *Hs*$DHODH_{33-396}$ protein solution (8.7 mg/mL) pre-equilibrated with 2 mM L-DHO, 2 mM **6**, 40 mM Zwitttergent 3-10, and 200 mM HEGA-8 by incubation on ice for 2 h. Both rat $DHODH_{23-396}$ and rat $DHODH_{33-396}$ were used for the random crystallization screen and optimization, but only rat $DHODH_{33-396}$ produced single crystals of diffraction quality. Crystals were obtained by mixing reservoir solution (1.64 M ammonium sulfate, 0.1 M sodium acetate, pH 4.2, 1.2 M NaCl, and 10 mM DTT) with an equal volume of the rat $DHODH_{33-396}$ protein solution (33 mg/mL) pre-equilibrated with 2 mM L-DHO, 2 mM **6**, and 80 mM HEGA-9 by incubation on ice for 2 h.

Structure Determination and Refinement. Crystals were flash frozen with liquid N_2 using immersion oil (type B) as a cryoprotectant, and diffraction data were collected at 100 K on beamline 19ID at Advanced Photon Source (APS) using an ADSC Q315 detector. Diffraction data were integrated, and intensities were scaled with the HKL2000 package.[35] Refinement statistics are shown in Supporting Information Table 1, and key ligand−protein distances are shown in Supporting Information Table 2. Crystallographic phases were solved by molecular replacement with Phaser[36] using previously reported structures. Bound ligands were removed from all search models prior to refinement. Structures were rebuilt with COOT[37] and refined with REFMAC.[38] Water molecules were added if the density was stronger than 3.4σ and removed if the density was weaker than 1σ in the density map with ARP/warp.[39] All residues in the three **6**−DHODH structures described below were within the allowed section of the Ramachandran plot.

Pf$DHODH_{\Delta384-413}$**−6** crystals diffracted to 2.1 Å in space group $P6_4$, with cell dimensions of $a = b = 85.5$ and $c = 138.3$. Crystallographic phases were solved by molecular replacement using PDB ID 3I65[15] and were refined to R and R_{free} of 0.185 and 0.240, respectively. Electron density for loop 348−354 was missing. The final structure contained 123 bound water molecules. *Hs*$DHODH_{33-396}$**−6** crystals diffracted to 1.25 Å in space group $P3_221$, with cell dimensions of $a = b = 90.9$ and $c = 121.1$. Crystallographic phases were solved by molecular replacement using PDB ID 4IGH[15,34] and refined to R and R_{free} of 0.141 and 0.156, respectively. Electron density for residues of 217−225 was missing. The final structure contained 368 bound water molecules. Rat $DHODH_{33-396}$**−6** crystals diffracted to 1.5 Å in space group $C2$, with cell dimensions of $a = 124.8$, $b = 43.9$, and $c = 63.1$. Crystallographic phases for rat $DHODH_{32-395}$**−6** were solved by molecular replacement using PDB ID 1UUO[40] and refined with REFMAC to R and R_{free} of 0.18 and 0.234, respectively. Electron density for residues 219−224 is missing. The final structure contained 126 bound water molecules. One molecule of DHODH was found in the asymmetric unit for all three structures. The coordinates for all three structures have been deposited in the Protein Data Bank (PDB) and are associated with the following codes: *Pf*DHODH−**6** (4ORM), *Hs*DHODH−**6** (4OQV), and rat DHODH−**6** (4ORI).

Structures were superimposed using the DaliLite program, and the rmsd was calculated from backbone atoms. Structures were displayed using PyMOL.[41]

Small Molecule X-ray Structure Determination. Structures were solved by standard methods, and a full description of crystallization methods and the refinement process can be found in the Supporting Information Methods. Refinement statistics are shown in Supporting Information Table 3. The coordinates for **6** (CCDC 986724) and **7** (CCDC 986723) have been deposited in the Cambridge Crystallographic Data Centre.

Isothermal Titration Calorimetry Analysis. ITC analyses were performed on a VP-ITC (MicroCal Inc.) at 30 °C in titration buffer (10 mM Hepes, pH 7.8, 20 mM NaCl, 5% glycerol, 1 mM LDAO, and 0.2% DMSO). *Pf*DHODH (5−10 μM) or rat DHODH (5−8 μM) were placed in the calorimetric cell and titrated with 50 μM inhibitor. Data were collected in triplicate and analyzed with NITPIC[42] and SEDPHAT (https://sedfitsedphat.nibib.nih.gov/software/default.aspx).

Enzyme Kinetic Analysis. The 50% inhibitory concentration (IC_{50}) was determined using either the DCIP dye-based assay or the direct assays as previously described[22,43] in assay buffer (100 mM Hepes, pH 8.0, 150 mM NaCl, 10% glycerol, and 0.1% Triton) plus 0.2 mM dihydroorotate (DHO) and 0.02 mM CoQ_D. For the DCIP-based assay, DCIP (0.12 mM) was included in the buffer, and absorbance was followed at 600 nm (ε = 18.8 mM^{-1} cm^{-1}). For the direct assay, buffer was supplemented with an O_2 depletion system that included 0.1 mg/mL glucose oxidase, 0.02 mg/mL catalase, and 50 mM glucose (incubated 5 min prior to assay), and orotic acid production was followed at 296 nM (ε_{296} = 4.3 M^{-1} cm^{-1}). Reactions were started by addition of DHODH (E_T = 2−10 nM) and monitored at 25 °C using the Synergy H1 (BioTek Inc.) plate reader. Initial rates were used to determine reaction velocity in the absence (v_o) and presence (v_i) of compound (tested over a range of 0.01−100 μM using a 3-fold dilution series). Data were collected in triplicate, and the measured v_i/v_o values were fitted to the log[I] versus response (three parameters) equation in GraphPad Prism to determine IC_{50}. For the determination of apparent $K_{m,app}$ and k_{cat}, reaction conditions were as above except that when the DHO concentration was varied (5−500 μM), the CoQ_D concentration was held at a constant 0.15 mM and when CoQ_D (2.5−150 uM) was varied, DHO was held fixed at 0.5 mM. For k_{cat} determination, protein concentration was determined by measuring flavin content at 454 nM (extinction coefficient = 11 cm^{-1} mM^{-1}). Data were fitted to the Michaelis−Menten equation in GraphPad Prism to determine the kinetic parameters.

***P. falciparum* Whole-Cell Assays.** *P. falciparum* was propagated in RPMI-1640 containing 0.5% albumax I as previously described.[20,22] For EC_{50} determination, parasites (0.19 mL of 0.5% parasitemia, 0.5% HCT) were plated into 96-well microtiter plates containing 10 μL compound or DMSO control. The last column of each plate was reserved for non-parasitized RBCs (0.5% HCT) to determine background fluorescence. Serial dilutions of compound stocks were prepared in 100% DMSO at 200× the final concentration. After 72 h of incubation, parasitized RBCs were quantitated by the SYBR Green method. 2× SYBR Green I solution (20 μL) in 1× PBS was mixed with 20 μL of parasites in 96-well plates and incubated for 20 min, after which time 160 μL of 1× PBS was added. Fluorescence was detected using a BD Biosciences Acurri C6 flow cytometer, and events were recorded within gates that encompassed all asexual growth stages of the *P. falciparum* intraerythrocytic life cycle. A minimum 50 000 total events were recorded per well. Background events determined from non-parasitized RBC controls were subtracted from final counts. All data were collected in triplicate.

Physicochemical Properties. Partition coefficients ($LogD_{pH7.4}$) were estimated by comparing their chromatographic retention properties to a set of standard compounds with known partition coefficients as previously described.[20]

pK_a Calculations. The pK_a of the bridging N1 nitrogen proton was calculated using the Pearson education site (http://www.pearsonmylabandmastering.com/northamerica/masteringchemistry/).

■ ASSOCIATED CONTENT

Supporting Information

Methods used for small molecule crystallography; tables of crystallographic refinement statistics, crystallographic distances, and steady-state kinetic analysis of *Hs*DHODH; density maps for the DHODH−inhibitor structures; DHODH sequence alignment; stereoalignment of *Pf*DHODH structures; representative ITC data; and small molecule ORTEP structures. This material is available free of charge via the Internet at http://pubs.acs.org.

■ AUTHOR INFORMATION

Corresponding Author

*Tel: (214) 645-6164. E-mail: margaret.phillips@UTSouthwestern.edu.

Notes

The authors declare no competing financial interest.

■ ACKNOWLEDGMENTS

The authors thank Drs. José Coteron, Maria Marco, and Jorge Esquivias (GlaxoSmithKline, Tres Cantos Medicines Development Campus, Madrid, Spain) for synthesis of **10**, Dr. Chad Brautigam (UT Southwestern) for discussions on ITC analysis, Ali Villanueva for technical assistance, and Dr. David Waterson (Medicines for Malaria Venture) for helpful comments on the manuscript. Protein crystallographic data were collected at the Advanced Photon Source Argonne National Laboratory (APS). The authors would like to thank the APS staff for their efforts. This work was supported by United States National Institutes of Health grants U01AI075594 (to M.A.P., P.K.R., and S.A.C.) and R01AI103947 (to M.A.P. and P.K.R.). M.A.P. also acknowledges the support of the Welch Foundation (I-1257), and P.K.R. is Program Director of the NIH South Asia ICEMR (AI089688). M.A.P. holds the Beatrice and Miguel Elias Distinguished Chair in Biomedical Science and the Carolyn R. Bacon Professorship in Medical Science and Education.

■ ABBREVIATIONS USED

*Pf*DHODH, *Plasmodium falciparum* dihydroorotate dehydrogenase; *Hs*DHODH, human DHODH; rDHODH, rat DHODH; mDHODH, mouse DHODH; dDHODH, dog DHODH; FMN, flavin mononucleotide; CoQ, ubiquinone; LDAO, *N*,*N*-dimethyldodecylamine *N*-oxide; DCIP, 2,6-dichloroindophenol

■ REFERENCES

(1) Miller, L. H.; Ackerman, H. C.; Su, X. Z.; Wellems, T. E. Malaria biology and disease pathogenesis: insights for new treatments. *Nat. Med.* **2013**, *19*, 156−67.

(2) Heppner, D. G. The malaria vaccine−status quo 2013. *Travel Med. Infect. Dis.* **2013**, *11*, 2−7.

(3) Olotu, A.; Fegan, G.; Wambua, J.; Nyangweso, G.; Awuondo, K. O.; Leach, A.; Lievens, M.; Leboulleux, D.; Njuguna, P.; Peshu, N.; Marsh, K.; Bejon, P. Four-year efficacy of RTS,S/AS01E and its interaction with malaria exposure. *N. Engl. J. Med.* **2013**, *368*, 1111−20.

(4) White, N. J. The role of anti-malarial drugs in eliminating malaria. *Malar J.* **2008**, *7*, S8.

(5) Eastman, R. T.; Fidock, D. A. Artemisinin-based combination therapies: a vital tool in efforts to eliminate malaria. *Nat. Rev. Microbiol.* **2009**, *7*, 864−74.

(6) Dondorp, A. M.; Ringwald, P. Artemisinin resistance is a clear and present danger. *Trends Parasitol.* **2013**, *29*, 359−60.

(7) Miotto, O.; Almagro-Garcia, J.; Manske, M.; Macinnis, B.; Campino, S.; Rockett, K. A.; Amaratunga, C.; Lim, P.; Suon, S.; Sreng, S.; Anderson, J. M.; Duong, S.; Nguon, C.; Chuor, C. M.; Saunders, D.; Se, Y.; Lon, C.; Fukuda, M. M.; Amenga-Etego, L.; Hodgson, A. V.; Asoala, V.; Imwong, M.; Takala-Harrison, S.; Nosten, F.; Su, X. Z.; Ringwald, P.; Ariey, F.; Dolecek, C.; Hien, T. T.; Boni, M. F.; Thai, C. Q.; Amambua-Ngwa, A.; Conway, D. J.; Djimde, A. A.; Doumbo, O. K.; Zongo, I.; Ouedraogo, J. B.; Alcock, D.; Drury, E.; Auburn, S.; Koch, O.; Sanders, M.; Hubbart, C.; Maslen, G.; Ruano-Rubio, V.; Jyothi, D.; Miles, A.; O'Brien, J.; Gamble, C.; Oyola, S. O.; Rayner, J. C.; Newbold, C. I.; Berriman, M.; Spencer, C. C.; McVean, G.; Day, N. P.; White, N. J.; Bethell, D.; Dondorp, A. M.; Plowe, C. V.; Fairhurst, R. M.; Kwiatkowski, D. P. Multiple populations of artemisinin-resistant *Plasmodium falciparum* in Cambodia. *Nat. Genet.* **2013**, *45*, 648−55.

(8) Fairhurst, R. M.; Nayyar, G. M.; Breman, J. G.; Hallett, R.; Vennerstrom, J. L.; Duong, S.; Ringwald, P.; Wellems, T. E.; Plowe, C. V.; Dondorp, A. M. Artemisinin-resistant malaria: research challenges, opportunities, and public health implications. *Am. J. Trop. Med. Hyg.* **2012**, *87*, 231−41.

(9) Ariey, F.; Witkowski, B.; Amaratunga, C.; Beghain, J.; Langlois, A. C.; Khim, N.; Kim, S.; Duru, V.; Bouchier, C.; Ma, L.; Lim, P.; Leang, R.; Duong, S.; Sreng, S.; Suon, S.; Chuor, C. M.; Bout, D. M.; Menard, S.; Rogers, W. O.; Genton, B.; Fandeur, T.; Miotto, O.; Ringwald, P.; Le Bras, J.; Berry, A.; Barale, J. C.; Fairhurst, R. M.; Benoit-Vical, F.; Mercereau-Puijalon, O.; Menard, D. A molecular marker of artemisinin-resistant *Plasmodium falciparum* malaria. *Nature* **2014**, *505*, 50−5.

(10) White, N. J. Antimalarial drug resistance. *J. Clin. Invest.* **2004**, *113*, 1084−92.

(11) Wells, T. N.; Alonso, P. L.; Gutteridge, W. E. New medicines to improve control and contribute to the eradication of malaria. *Nat. Rev. Drug Discovery* **2009**, *8*, 879−91.

(12) Burrows, J. N.; Hooft van Huijsduijnen, R.; Mohrle, J. J.; Oeuvray, C.; Wells, T. N. Designing the next generation of medicines for malaria control and eradication. *Malar. J.* **2013**, *12*, 187.

(13) Phillips, M. A.; Rathod, P. K. *Plasmodium* dihydroorotate dehydrogenase: a promising target for novel anti-malarial chemotherapy. *Infect. Disord.: Drug Targets* **2010**, *10*, 226−39.

(14) Booker, M. L.; Bastos, C. M.; Kramer, M. L.; Barker, R. H., Jr.; Skerlj, R.; Bir Sdhu, A.; Deng, X.; Celatka, C.; Cortese, J. F.; Guerrero Bravo, J. E.; Krespo Llado, K. N.; Serrano, A. E.; Angulo-Barturen, I.; Belén Jiménez-Díaz, M.; Viera, S.; Garuti, H.; Wittlin, S.; Papastogiannidis, P.; Lin, J.; Janse, C. J.; Khan, S. M.; Duraisingh, M.; Coleman, B.; Goldsmith, E. J.; Phillips, M. A.; Munoz, B.; Wirth, D. F.; Klinger, J. D.; Wiegand, R.; Sybertz, E. Novel inhibitors of *Plasmodium falciparum* dihydroorotate dehydrogenase with anti-malarial activity in the mouse model. *J. Biol. Chem.* **2010**, *285*, 33054−33064.

(15) Deng, X.; Gujjar, R.; El Mazouni, F.; Kaminsky, W.; Malmquist, N. A.; Goldsmith, E. J.; Rathod, P. K.; Phillips, M. A. Structural plasticity of malaria dihydroorotate dehydrogenase allows selective binding of diverse chemical scaffolds. *J. Biol. Chem.* **2009**, *284*, 26999−27009.

(16) Hurt, D. E.; Widom, J.; Clardy, J. Structure of *Plasmodium falciparum* dihydroorotate dehydrogenase with a bound inhibitor. *Acta Crystallogr., Sect. D: Biol. Crystallogr.* **2006**, *62*, 312−23.

(17) Liu, S.; Neidhardt, E. A.; Grossman, T. H.; Ocain, T.; Clardy, J. Structures of human dihydroorotate dehydrogenase in complex with antiproliferative agents. *Structure* **2000**, *8*, 25−33.

(18) Munier-Lehmann, H.; Vidalain, P. O.; Tangy, F.; Janin, Y. L. On dihydroorotate dehydrogenases and their inhibitors and uses. *J. Med. Chem.* **2013**, *56*, 3148−67.

(19) Oh, J.; O'Connor, P. W. Teriflunomide for the treatment of multiple sclerosis. *Semin. Neurol.* **2013**, *33*, 45−55.
(20) Coteron, J. M.; Marco, M.; Esquivias, J.; Deng, X.; White, K. L.; White, J.; Koltun, M.; El Mazouni, F.; Kokkonda, S.; Katneni, K.; Bhamidipati, R.; Shackleford, D. M.; Angulo-Barturen, I.; Ferrer, S. B.; Jimenez-Diaz, M. B.; Gamo, F. J.; Goldsmith, E. J.; Charman, W. N.; Bathurst, I.; Floyd, D.; Matthews, D.; Burrows, J. N.; Rathod, P. K.; Charman, S. A.; Phillips, M. A. Structure-guided lead optimization of triazolopyrimidine-ring substituents identifies potent *Plasmodium falciparum* dihydroorotate dehydrogenase inhibitors with clinical candidate potential. *J. Med. Chem.* **2011**, *54*, 5540−5561.
(21) Gujjar, R.; El Mazouni, F.; White, K. L.; White, J.; Creason, S.; Shackleford, D. M.; Deng, X.; Charman, W. N.; Bathurst, I.; Burrows, J.; Floyd, D. M.; Matthews, D.; Buckner, F. S.; Charman, S. A.; Phillips, M. A.; Rathod, P. K. Lead-optimization of aryl and aralkyl amine based triazolopyrimidine inhibitors of *Plasmodium falciparum* dihydroorotate dehydrogenase with anti-malarial activity in mice. *J. Med. Chem.* **2011**, *54*, 3935−49.
(22) Gujjar, R.; Marwaha, A.; El Mazouni, F.; White, J.; White, K. L.; Creason, S.; Shackleford, D. M.; Baldwin, J.; Charman, W. N.; Buckner, F. S.; Charman, S.; Rathod, P. K.; Phillips, M. A. Identification of a metabolically stable triazolopyrimidine-based dihydroorotate dehydrogenase inhibitor with antimalarial activity in mice. *J. Med. Chem.* **2009**, *52*, 1864−72.
(23) Marwaha, A.; White, J.; El Mazouni, F.; Creason, S. A.; Kokkonda, S.; Buckner, F. S.; Charman, S. A.; Phillips, M. A.; Rathod, P. K. Bioisosteric transformations and permutations in the triazolopyrimidine scaffold to identify the minimum pharmacophore required for inhibitory activity against *Plasmodium falciparum* dihydroorotate dehydrogenase. *J. Med. Chem.* **2012**, *55*, 7425−36.
(24) Phillips, M. A.; Gujjar, R.; Malmquist, N. A.; White, J.; El Mazouni, F.; Baldwin, J.; Rathod, P. K. Triazolopyrimidine-based dihydroorotate dehydrogenase inhibitors with potent and selective activity against the malaria parasite *Plasmodium falciparum*. *J. Med. Chem.* **2008**, *51*, 3649−3653.
(25) Muller, K.; Faeh, C.; Diederich, F. Fluorine in pharmaceuticals: looking beyond intuition. *Science* **2007**, *317*, 1881−6.
(26) Zhou, P.; Zou, J.; Tian, F.; Shang, Z. Fluorine bonding−how does it work in protein-ligand interactions? *J. Chem. Inf. Model.* **2009**, *49*, 2344−55.
(27) Ottaviani, P.; Caminati, W.; Favero, L. B.; Blanco, S.; Lopez, J. C.; Alonso, J. L. Molecular beam rotational spectrum of cyclobutanone-trifluoromethane: nature of weak CH···O═C and CH···F hydrogen bonds. *Chemistry* **2006**, *12*, 915−20.
(28) Alonso, J. L.; Antolinez, S.; Blanco, S.; Lesarri, A.; Lopez, J. C.; Caminati, W. Weak C-H···O and C-H···F-C hydrogen bonds in the oxirane-trifluoromethane dimer. *J. Am. Chem. Soc.* **2004**, *126*, 3244−9.
(29) Buer, B. C.; Marsh, E. N. Fluorine: a new element in protein design. *Protein Sci.* **2012**, *21*, 453−62.
(30) Weeks, A. M.; Coyle, S. M.; Jinek, M.; Doudna, J. A.; Chang, M. C. Structural and biochemical studies of a fluoroacetyl-CoA-specific thioesterase reveal a molecular basis for fluorine selectivity. *Biochemistry* **2010**, *49*, 9269−79.
(31) Rathod, P. K.; Floyd, D.; Burrows, J.; Marwaha, A.; Gujjar, R.; Coteron-Lopez; Phillips, M. A.; Charman, S.; Matthews, D. Antimalarial agents that are inhibitor of dihydroorotate dehydrogenase. World Intellectual Property Organization, Patent WO 2011/041304, 2011.
(32) Baldwin, J.; Michnoff, C. H.; Malmquist, N. A.; White, J.; Roth, M. G.; Rathod, P. K.; Phillips, M. A. High-throughput screening for potent and selective inhibitors of *Plasmodium falciparum* dihydroorotate dehydrogenase. *J. Biol. Chem.* **2005**, *280*, 21847−21853.
(33) Patel, V.; Booker, M.; Kramer, M.; Ross, L.; Celatka, C. A.; Kennedy, L. M.; Dvorin, J. D.; Duraisingh, M. T.; Sliz, P.; Wirth, D. F.; Clardy, J. Identification and characterization of small molecule inhibitors of *Plasmodium falciparum* dihydroorotate dehydrogenase. *J. Biol. Chem.* **2008**, *283*, 35078−85.
(34) Das, P.; Deng, X.; Zhang, L.; Roth, M. G.; Fontoura, B. M.; Phillips, M. A.; De Brabander, J. K. SAR based optimization of a 4-quinoline carboxylic acid analog with potent anti-viral activity. *ACS Med. Chem. Lett.* **2013**, *4*, 517−521.
(35) Otwinowski, Z.; Minor, W. Processing of X-ray diffraction data collected in oscillation mode. *Method Enzymol.* **1997**, *276*, 307−326.
(36) McCoy, A. J. Solving structures of protein complexes by molecular replacement with Phaser. *Acta Crystallogr., Sect. D: Biol. Crystallogr.* **2007**, *63*, 32−41.
(37) Emsley, P.; Cowtan, K. Coot: model-building tools for molecular graphics. *Acta Crystallogr., Sect. D: Biol. Crystallogr.* **2004**, *60*, 2126−32.
(38) Murshudov, G. N.; Vagin, A. A.; Dodson, E. J. Refinement of macromolecular structures by the maximum-likelihood method. *Acta Crystallogr., Sect. D: Biol. Crystallogr.* **1997**, *53*, 240−55.
(39) Kleywegt, G. J.; Jones, T. A. A super position. *CCP4/ESF-EACBM Newsletter on Protein Crystallography*, 1994; Vol. *31*, pp 9−14.
(40) Hansen, M.; Le Nours, J.; Johansson, E.; Antal, T.; Ullrich, A.; Loeffler, M.; Larsen, S. Inhibitor binding in a class 2 dihydroorotate dehydrogenase causes variations in the membrane-associated N-terminal domain. *Protein Sci.* **2004**, *13*, 1031−1042.
(41) *PyMOL Molecular Graphics System*; DeLano Scientific: San Carlos, CA, 2000.
(42) Keller, S.; Vargas, C.; Zhao, H.; Piszczek, G.; Brautigam, C. A.; Schuck, P. High-precision isothermal titration calorimetry with automated peak-shape analysis. *Anal. Chem.* **2012**, *84*, 5066−73.
(43) Malmquist, N. A.; Gujjar, R.; Rathod, P. K.; Phillips, M. A. Analysis of flavin oxidation and electron-transfer inhibition in *Plasmodium falciparum* dihydroorotate dehydrogenase. *Biochemistry* **2008**, *47*, 2466−75.
(44) March, J. *March's Advanced Organic Chemistry: Reactions, Mechanisms, and Structure*, 4th ed.; Wiley India Pvt Ltd: Hoboken, NJ, 2006.